

Evaluation of polarization mode dispersion in a telecommunication wavelength selective switch using quantum interferometry

A. Fraine,^{1,*} O. Minaeva,² D. S. Simon,^{1,3} R. Egorov,¹ and A. V. Sergienko^{1,2,4}

¹*Dept. of Electrical and Computer Engineering, Boston University, 8 Saint Mary's St., Boston, MA 02215, USA*

²*Dept. of Biomedical Engineering, Boston University, 44 Cummings St., Boston, MA 02215, USA*

³*Dept. of Physics and Astronomy, Stonehill College, 320 Washington St., Easton, MA 02357, USA*

⁴*Dept. of Physics, Boston University, 590 Commonwealth Ave., Boston, MA 02215, USA*

[*afraine@bu.edu](mailto:afraine@bu.edu)

Abstract: A polarization mode dispersion (PMD) measurement of a commercial telecommunication wavelength selective switch (WSS) using a quantum interferometric technique with polarization-entangled states is presented. Polarization-entangled photons with a broad spectral width covering the telecom band are produced using a chirped periodically poled nonlinear crystal. The first demonstration of a quantum metrology application using an industrial commercial device shows a promising future for practical high-resolution quantum interference.

© 2012 Optical Society of America

OCIS codes: (270.0270) Quantum optics; (120.3180) Interferometry; (120.3940) Metrology; (260.2030) Dispersion.

References and links

1. C. K. Hong, Z. Y. Ou, and L. Mandel, "Measurement of subpicosecond time intervals between two photons by interference," *Phys. Rev. Lett.* **18**, 2044–2046 (1987).
2. A. V. Sergienko, Y. H. Shih, M. H. Rubin, "Experimental evaluation of a two-photon wave packet in type-II parametric downconversion," *J. Opt. Soc. Am. B* **12**, 859–862 (1995).
3. D. Branning, A. L. Migdall, and A. V. Sergienko, "Simultaneous measurement of group and phase delay between two photons," *Phys. Rev. A* **62**, 063808 (2000).
4. E. Dauler, G. Jaeger, A. Muller, A. L. Migdall, and A. V. Sergienko, "Tests of a two-photon technique for measuring polarization mode dispersion with subfemtosecond precision," *J. Res. Natl. Inst. Stand. Technol.* **104**, 1–10 (1999).
5. A. Fraine, D. S. Simon, O. Minaeva, R. Egorov, and A. V. Sergienko, "Precise evaluation of polarization mode dispersion by separation of even- and odd-order effects in quantum interferometry," *Opt. Express* **19**, 22820–22836 (2011).
6. S. Diddams and J. Diels, "Dispersion measurements with white-light interferometry," *J. Opt. Soc. Am. B* **13**, 1120–1129 (1996).
7. Y. Namihira, K. Nakajima, and T. Kawazawa, "Fully automated interferometric PMD measurements for active EDFA, fibre optic components and optical fibres," *Electron. Lett.* **29**, 1649–1651 (1993).
8. B. L. Heffner, "Accurate, automated measurement of differential group delay dispersion and principal state variation using jones matrix eigenanalysis," *IEEE Photon. Technol. Lett.* **5**, 814–817(1993).
9. P. Williams, "PMD measurement techniques and how to avoid the pitfalls," *J. Opt. Fiber Commun.* **Rep. 1**, 84–105 (2004).

10. P. G. Kwiat, K. Mattle, H. Weinfurter, A. Zeilinger, A. V. Sergienko, and Y. H. Shih, "New high intensity source of polarization-entangled photon pairs," *Phys. Rev. Lett.* **75**, 4337–4341 (1995).
 11. M. Charbonneau-Lefort, B. Afeyan, and M. M. Fejer, "Optical parametric amplifiers using chirped quasi-phase-matching gratings I: practical design formulas," *J. Opt. Soc. Am. B* **25**, 463–480 (2008).
 12. M. Nasr, S. Carrasco, B. Saleh, A. V. Sergienko, and M. C. Teich, J. P. Torres, L. Torner, D. Hum, M. M Fejer, "Ultrabroadband biophotons generated via chirped quasi-phase-matched optical parametric down-conversion," *Phys. Rev. Lett.* **100**, 183601 (2005).
 13. S. Carrasco, J. P. Torres, L. Torner, A. V. Sergienko, B. Saleh, and M. C. Teich, "Enhancing the axial resolution of quantum optical coherence tomography by aperiodic quasi-phase-matching," *Opt. Lett.* **29**, 2429–2431 (2004).
 14. M. H. Rubin, D. N. Klyshko, Y. H. Shih, and A. V. Sergienko, "Theory of two-photon entanglement in type-II optical parametric down-conversion," *Phys. Rev. A* **50**, 5122–5133 (1994).
 15. Capella Intelligent Subsystems Inc., "Capella CR50," <http://www.capellainc.com/products/CR50/index.htm>.
 16. G. N. Gol'tsman, O. Okunev, G. Chulova, A. Lipatov, A. Semenov, K. Smirnov, B. Voronov, A. Dzardanov, C. Williams, and R. Sobolewski, "Picosecond superconducting single-photon optical detector," *Appl. Phys. Lett.* **79**, 705–707 (2001).
 17. S. Emanueli and A. Arie, "Temperature-dependent dispersion equations for KTiOPO_4 and KTiOAsO_4 ," *Appl. Opt.* **42**, 6661–6665 (2003).
-

1. Introduction

The need for high-resolution dispersion measurements is increasing with current trends in high-speed fiber optic networks. The evaluation of dispersion parameters from discrete components such as optical switches is critical for the overall system performance. In particular, it is desirable to measure extremely small (<1 fs) values of polarization mode dispersion (PMD). Until the widespread deployment of ROADM (reconfigurable optical add-drop multiplexer) systems, only fiber PMD was considered to be a major contributor to the overall system PMD. With an increase in the transmission bit rate, the aggregate effect of discrete component PMD is becoming comparable to the PMD introduced by the fiber.

The advantages of using quantum interference to measure short time delays between two photons was recognized in the early days of quantum optics [1, 2]. In particular, the use of quantum interferometry with polarization-entangled states has been shown to provide an accurate measurement of PMD [3–5] that has the potential to go beyond the limitations of classical techniques such as white light interferometry [6, 7] and the Jones Matrix Eigenanalysis (JME) method [8, 9]. Quantum interference has also been shown to be more stable than classical interferometric methods due to the fourth order interference of intensities rather than the second order interference of electric fields making it less sensitive to environmental changes [4]. It was shown that uncertainties of 0.1 fs for group delay and 2 attoseconds for phase delay can be reached using quantum interferometry without any sophisticated stabilization efforts [3]. The result reported here is the first practical application of quantum interferometry that paves the way for high-resolution evaluation of PMD in real-world discrete telecommunication devices.

The ultimate resolution of interferometric measurements relies heavily on the spectral bandwidth of the source. The type-II spontaneous parametric down conversion (SPDC) [10] has been a common source of choice for the generation of polarization-entangled states. However, the spectral bandwidth of polarization-entangled photons generated using type-II phase matching in bulk nonlinear crystals is naturally not very broad. Previous demonstrations of high-resolution quantum interferometry used very thin BBO crystals to produce broadband down converted photons that naturally resulted in low intensities. The introduction of periodically poled crystals as sources of down conversion photons allowed more flexibility in designing specific phase matching profiles. Chirped periodically poled crystals have been studied in detail for broadband optical parametric amplifiers [11] as well as for type-I spontaneous parametric down conversion for high resolution OCT measurements [12, 13]. It has been shown that chirped periodically poled nonlinear structures are capable of manipulating the output spectrum that ultimately defines the resolution of the quantum interference technique. A type-II linearly chirped period-

ically poled crystal is used here as a broadband source of polarization-entangled photons. Some specifics of type-II parametric down conversion in a chirped nonlinear crystal will be discussed in detail elsewhere.

2. Theory

The overall spectrum of down conversion radiation generated from multiple nonlinear layers of periodically poled crystals is proportional to the Fourier transform of the nonlinear coefficient given by

$$\tilde{\chi}^{(2)}(\omega_s, \omega_p - \omega_s) = \chi_0 \sum_{j=1}^N (-1)^j L_j \text{sinc}(L_j \Delta k / 2) e^{-i\Delta k(L_j/2 + \sum_{k=j+1}^N L_k)} \quad (1)$$

where $\Delta k = \Delta k(\omega_s, \omega_p - \omega_s) = k_p(\omega_p) - k_s(\omega_s) - k_i(\omega_p - \omega_s)$, ω_s and ω_p are the signal and pump frequencies respectively, and L_j is the length of the j^{th} single crystal emitter given by $L_j = \frac{p_0}{2} (1 + \frac{\Delta p}{L_c} (z_j - z_0))$ for a linearly chirped crystal shown in Fig. 1. The design parameters include p_0 as the degenerate type-II collinear phase matching period, L_c as the total length of the crystal, z_0 and z_j as the location of p_0 and the j^{th} single crystal emitter respectively, and Δp as the amount of chirping in the system ($\Delta p = 0$ for no chirp, $\Delta p = 0.5$ for 50% chirp). This function can be understood as a superposition of contributions from thin crystals of varying lengths distributed along the axis of propagation. Each contribution consists of a $\text{sinc}(L_j \Delta k / 2)$ spectral function along with the appropriate phase determined by the location of the emitter. The two-photon state from the spontaneous parametric down conversion is written as [2, 14]:

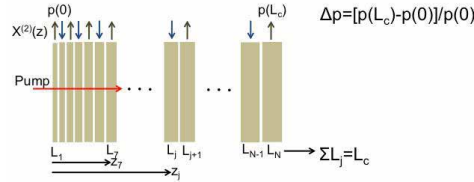


Fig. 1. Linearly chirped nonlinear crystal.

$$|\Psi\rangle = \int d\omega \tilde{\chi}^{(2)}(\omega, \omega_p - \omega) \hat{a}_H^\dagger(\omega) \hat{a}_V^\dagger(\omega_p - \omega) |0\rangle. \quad (2)$$

By sending this state into a polarization quantum interferometer shown in Fig. 2 and described in [3–5], a post-selected polarization-entangled state of the form $|\Psi\rangle = (|H, V\rangle - |V, H\rangle) / \sqrt{2}$ is extracted through coincidence detection. In one arm, a birefringent delay line delays one polarization mode relative to the other. In front of each detector an analyzer at $\pm 45^\circ$ insures indistinguishability between polarization states. The coincidence rate of the form $R(L_b) = C(R_0 - R_{int}(L_b))$ is given by

$$R_0 = \int d\omega |\tilde{\chi}^{(2)}(\omega, \omega_p - \omega)|^2 \quad (3)$$

$$R_{int}(L_b) = \int d\omega \tilde{\chi}^{(2)}(\omega, \omega_p - \omega) \tilde{\chi}^{(2)*}(\omega_p - \omega, \omega) \times [e^{i(\Delta n_b(\omega)\omega L_b/c + \Delta k_s(\omega)L_s)} + e^{i(\Delta n_b(\omega_p - \omega)(\omega_p - \omega)L_b/c + \Delta k_s(\omega_p - \omega)L_s)}] \quad (4)$$

where $\Delta n_b(\omega)$ is the difference between the signal and idler indices of refraction at frequency ω in the birefringent delay line, Δk_s is the differential dispersion in the sample, L_b is the length of

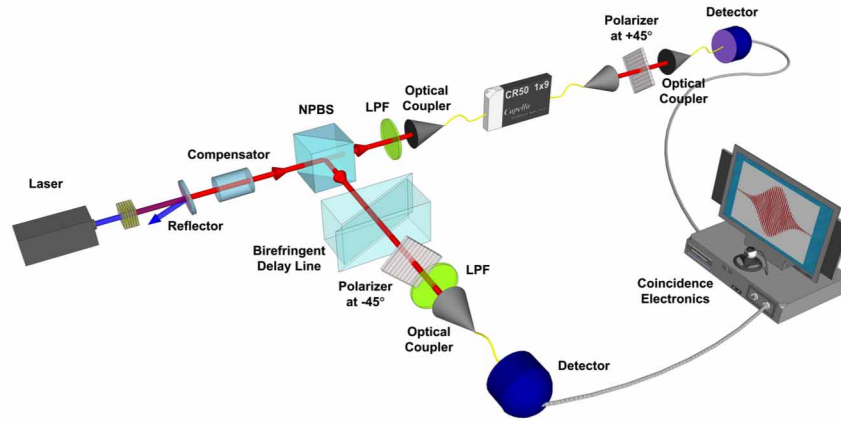


Fig. 2. Setup for PMD measurement. Radiation from a Ti:Sapphire laser at 775nm pumps a linearly chirped PPKTP crystal to produce broadband type-II SPDC. The photon pairs propagate through a birefringent compensating element and enter a non-polarizing beam splitter. One arm contains the sample under test and the other contains a birefringent delay line. The photons are collected after traveling through crossed polarizers at $\pm 45^\circ$ and detected in coincidence with two superconducting single photon detectors.

the birefringent delay line, and L_s is the length of the sample. By measuring the shift in the interference feature of the coincidence rate whose shape is defined by the spectrum, the differential group delay of the sample given by $\Delta\tau = \Delta k_s(\omega_0)L_s/\omega_0 = \Delta NL_s/c$ can be extracted where ΔN is the difference in the group index of refraction between signal and idler polarizations in the sample, and ω_0 is the central frequency of the down conversion source.

3. Experiment

To demonstrate the practical use of quantum interferometry for high resolution PMD measurements, we measure the differential group delay from a wavelength selective switch (WSS) [15]. In this configuration, a WSS admits a broad spectrum consisting of 96 possible wavelength channels (50 GHz width) in a single input fiber. A diffraction grating disperses the signal onto a configurable MEMS mirror array with one pixel assigned to each wavelength channel. Each pixel can then redirect a specific wavelength to an any of the nine output fibers. The prevalence of these devices in fiber communication networks makes it a relevant sample to demonstrate the use of quantum interferometry for PMD evaluation. Even though each individual switch is assumed to have small PMD, the combined effect of many switches in a network may significantly contribute to the overall system PMD.

In addition, a sample with a known differential group delay and length was measured for calibration and demonstration of the resolution capability. We exploit the properties of collinear type-II spontaneous parametric down conversion from a linearly chirped PPKTP crystal with $\Delta p = 0.5$, $z_0 = L_c/2$, at $T = 125^\circ C$. The correlated orthogonally polarized pairs centered around 1550 nm with a bandwidth of approximately 125 nm are created by pumping the chirped periodically poled nonlinear crystal (PPKTP) situated in a temperature stabilized oven with a radiation of Ti:Sapphire laser in a CW regime at 775 nm. After propagating through a birefringent compensator, non-polarizing beam splitter, and polarizers crossed at 45 degrees, the collected signals are sent to two superconducting NbN nanowire single-photon detectors [16] and the

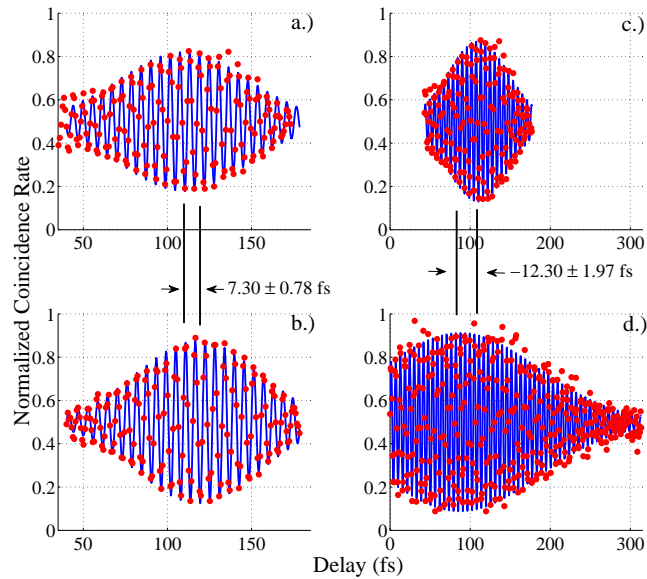


Fig. 3. Comparison of interferograms (red circles) before (a,c) and after (b,d) the sample is introduced yields the differential group delay. (a,b) Calibration of the measurement device with a known sample producing a shift of $\Delta\tau = 7.30 \pm 0.80$ fs agreeing closely with the expected value of $\Delta\tau = 7.31 \pm 0.01$ fs. The differential group delay of the WSS is obtained from comparing c.) and d.). The Gaussian fits (blue lines) have goodness of fit parameters of $R^{(2)} = 0.975$ and $R^{(2)} = 0.959$ respectively.

coincidence rate is measured between the two detectors as a function of the birefringent delay. A sample placed in one of the arms of such an entangled-photon polarization interferometer shifts the interference feature, enabling the evaluation of the differential group delay.

To calibrate the performance of such a device, a sample with a well known differential group delay was measured (see Figs. 3a, 3b). This measurement demonstrates the capability of the measurement apparatus when the sample has no spectral limitations and can accommodate the full spectral bandwidth of polarization entanglement. The known sample is a 71.84 ± 0.10 μm long BBO crystal cut at $\theta = 29.5^\circ$ resulting in an expected shift of $\Delta\tau = 7.31 \pm 0.01$ fs. The experimental observation coincides with the expected delay within ± 0.01 fs.

When a sample having specific spectral constraints such as a WSS is evaluated ($\Delta\lambda = 96$ channels \times 0.4 nm ≈ 38.4 nm), one must take into account a deterministic fixed offset in the position of the interference envelope center of mass due to specific filtering of the original entangled state spectrum ($\Delta\lambda = 125$ nm) by the sample. The overall shift due to spectral filtering inside the WSS was calibrated using an independent interference filter of a similar spectral width ($\Delta\lambda = 40$ nm) centered around 1550 nm. This ensures an accurate numerical determination of the fixed shift of the interference envelope center due to the known sub-selection of the original broad spectrum by the sample. Although this procedure introduces an extra source of uncertainty in the PMD measurement, this step is necessary to distinguish the genuine differential group delay of the sample from the shift due to spectral modification.

The PMD of the switch is extracted by analyzing the experimentally observed shift of the interferogram after the introduction of the WSS in one arm of the interferometer and taking

into account the spectrally induced shift. The two scans are shown in Fig. 3c and Fig. 3d, displaying the PMD of one particular output port. The observed shift without the introduction of the spectrally-induced part is $\Delta\tau_0 = -12.30 \pm 1.97$ fs. Including the spectral shift of $\Delta\tau_S = -24.93 \pm 1.97$ fs, the overall PMD of the WSS is $\Delta\tau_0 = 24.93 - 12.30 = 12.63 \pm 3.75$ fs. Multiple measurements have shown that slight PMD value variations exist between the 9 output ports, likely due to minor differences in optical paths and differences in fiber output assemblies.

Both sets of data are fit with a function of the form $R(\tau) = Ce^{-(\tau-\tau_0)^2/\Delta\tau^2} \sin(2\pi\nu\tau + \phi) + R_0$ to locate the point of maximum interference, τ_0 . An estimation of the uncertainty in the measurement is determined by considering the statistical variation of τ_0 derived from several measurements resulting in a statistical uncertainty of $\sigma_{\tau_S} = 1.97$ fs. Considering the uncertainty originating from the numerical estimation of the fixed spectral shift which produces a discrepancy of $\sigma_{\tau_N} = 2.51$ fs between simulation and experiment and the uncertainty of the experimental evaluation of the known filter $\sigma_{\tau_F} = 1.97$ fs, an estimate of the overall uncertainty in the measurement is $\sigma_{\tau_0} = \sqrt{\sigma_{\tau_S}^2 + \sigma_{\tau_N}^2 + \sigma_{\tau_F}^2} = 3.75$ fs. The temperature derivatives of the index of refraction [17] used for the phase-matching calculation in the numerical determination of the spectral shift is likely the source of error responsible for σ_{τ_N} . There are several reports on such coefficients that appear to be in disagreement as discussed in [17] which can easily be responsible for shifts on the order of 1 fs when comparing the numerical simulation with the experimental realization.

Since the PMD fluctuates from one output port of the WSS to another, an overall PMD value for the device does not provide a full picture; therefore, based on measurements from several output ports, a conservative evaluation of an upper bound for the PMD of this particular switch is $|\Delta\tau_0| < 30$ fs.

4. Comparison of classical and quantum interference

To demonstrate the practical difference between classical and quantum interference for the evaluation of PMD, the classical polarization interferometer shown in Fig. 4 was implemented in the same experimental conditions as the quantum measurements previously discussed.

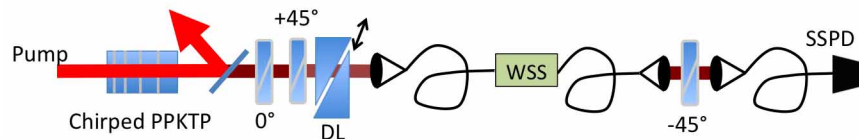


Fig. 4. Classical polarization interferometer. A classical “white light” source of the same spectral bandwidth is constructed by selecting only one horizontal component of the SPDC source. It is introduced into a polarization Mach-Zehnder interferometer. A projection onto the 45° basis is formed with a first polarizer and sent through the delay line (DL) aligned with the $0^\circ/90^\circ$ basis followed by the sample (WSS). The delay line and the sample decompose the 45° polarized light which is then recombined on a second -45° polarizer where the interference can occur. The signal is then coupled and sent to a single SSPD detector where the intensity is recorded as a function of the birefringent delay.

This is a polarization analogue to the traditional Mach-Zehnder interferometer that enjoys the highest stability due to the single-path nature of the setup. All other types of classical multiple-path interferometers will be even less stable.

The PMD of the known BBO sample using classical interferometry was found to be

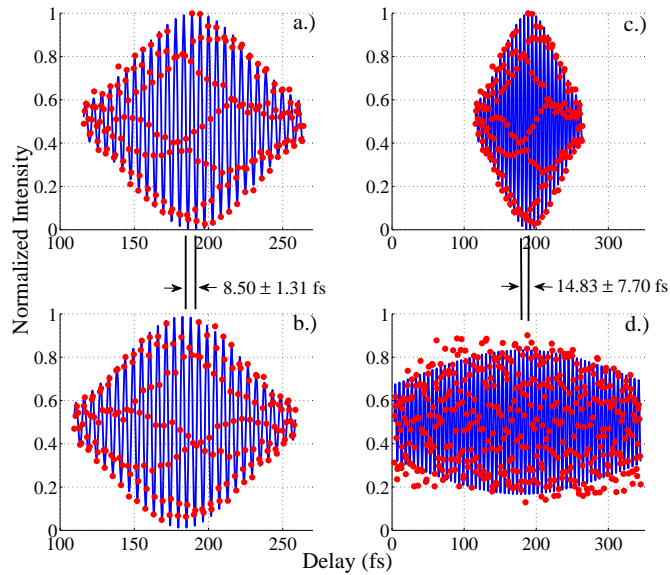


Fig. 5. The analogous measurements to those shown in Fig. 3 with the classical interferometer of Fig. 4. The known calibration birefringent sample revealed a PMD of $\Delta\tau = 7.80 \pm 1.31$ fs (a,b). The measurement of the WSS, obscured by weak scattering (<1 pW) from an internal light source entering the output fibers, revealed a PMD of $\Delta\tau = 14.83 \pm 7.73$ fs displayed in (c,d) with background correction. The goodness of fit parameters for (c) and (d) are $R^{(2)} = 0.989$ and $R^{(2)} = 0.930$ respectively for the fitting function described in Section 3.

$\Delta\tau = 7.80 \pm 1.31$ fs and $\Delta\tau = 14.83 \pm 7.73$ fs for the WSS (see Fig. 5). The similar quantum measurement (Fig. 3) of the calibration sample was closer to the expected value and had much smaller uncertainty. With exactly the same experimental conditions in terms of equipment, measurement procedure, and environmental considerations, an explanation for the advantage of the quantum interferometer is the increased fringe stability due to the use of fourth order interference of intensities in the quantum case rather than the second order interference of electric fields in the classical interferometer. The classical PMD measurement of the real telecommunication WSS (Figs. 3c, 3d) was affected by the existence of some internal source of light that is usually used for active monitoring and alignment of WSS optical elements and mechanisms. The overall amount of light that is scattered into the output fibers of the switch is extremely low (<1 pW) and does not affect classical communication channels that operate with powers on the order of 1 mW. However, when a weak source such as SPDC is used, the noise from inside the device is comparable to the signal of interest in our measurement scheme. A comparison of interferograms before background correction in the classical and quantum cases is shown in Fig. 6. This problem is naturally eliminated in the quantum interferometer due to correlated detection, highlighting the fact that only correlated photons from the SPDC process contribute in coincidence despite the relatively large amount of scattered light detected in singles from the switch. Correlated detection results in a much higher signal to noise ratio even in the presence of ambient noise. Although this problem in the classical case could be solved by using a stronger source, it has been proven quite difficult to make such broadband (>120 nm) and uniform classical light source without sharp spectral features in this wavelength range. This

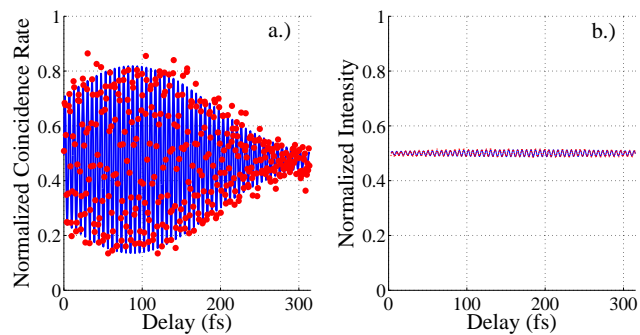


Fig. 6. Comparison of quantum (a) and classical (b) interferograms through the WSS before background correction. It is clear that quantum interferometry has an extra benefit of correlated detection that provides a measurement immune to reasonable levels of uncorrelated noise in the system.

is why SPDC from chirped periodically poled crystals is a convenient source of light for this application. It is not difficult to significantly broaden the spectrum of SPDC beyond the current bandwidth of 125 nm with this type of source by simply increasing the amount of chirping in the crystal which will be discussed in detail elsewhere.

In the case of classical interferometry, filtering will not have the same shifting effect as in the quantum case. Classical interference is between two polarization modes with the same original spectrum that always achieve maximum indistinguishability when there is zero delay between polarization components. In the case of quantum interference, a filter can modify the distinguishable spectra of each polarization such that the temporal delay that creates the highest degree of indistinguishability can depend on the specific sub-selection of the spectra by the filter.

In summary, quantum interferometry appears to enjoy greater fringe stability due to coincidence detection where the interference is essentially observed in the coincidence circuit. Classical interferometry relies on the spatial overlap of electric fields which can be quite sensitive to environmental perturbations even in the most stable single path configuration described in this work. In addition, the nature of coincidence detection with a correlated source is more immune to noise from internal sources in telecommunication devices. Finally, a convenient and controllable source of broadband quantum states of light that can conceivably exceed 200 nm can be found from linearly chirped periodically poled crystals. These structures have the potential to considerably outperform current broadband sources due to the flexibility of phase-matching engineering.

5. Discussion

The ultimate resolution of the quantum interference technique is best realized when dealing with samples without spectral limitations. For example, a separate evaluation of a particular element used inside the switch such as the MEMS array may be a useful measurement for future applications. In addition, a comparison of a WSS based on MEMS technology with one based on LCOS (liquid crystal on silicon) technology may reveal significant advantages in terms of PMD performance due to the fundamentally birefringent nature of the LCOS device.

To overcome the complications initiated from spectrally limiting samples and to avoid the reliance on numerical evaluation of a fixed offset, the intelligent design of periodically poled crystals with more sophisticated grating patterns will be useful. Creating polarization-entangled

states with smooth and symmetric spectral shapes exactly matching the spectral width and center of mass of the device under test could improve this measurement resolution to the attosecond range by eliminating a sample-induced spectral filtering. There have been attempts to engineer smooth spectra from periodically poled structures specifically in OPA processes [11], but not for the correlated-photon applications of type-II SPDC. In addition, techniques such as engineering the spectral phases distributed along the crystal by alternating between poled and non-poled segments and an iterative technique that calculates a nonlinear chirping polynomial based on an initial condition of the desired spectrum could be viable solutions. Previous demonstrations of high resolution quantum interferometric PMD measurements have been shown to measure the group delay with a resolution of 0.1 fs [3] despite the extremely low intensities and absence of temperature and mechanical stabilization techniques. With a high intensity broadband source of polarization-entangled states, it would be conceivable to achieve a resolution of 10 attoseconds for the evaluation of differential group delay.

In comparison with the use of classical white light interferometry for PMD evaluation, the quantum interferometer enjoys a practical advantage in stability due to the fourth order intensity interference where the correlation is effectively evaluated in the coincidence circuit. In addition, the role of the invariance of polarization-entangled states to unitary transformations such as basis rotations must be investigated in comparison with classical techniques. Lastly, smooth broadband classical sources of white light are difficult to create and the most common sources are LEDs with bandwidths not exceeding 80 nm. The ability to specially tailor the down conversion spectrum from periodically poled structures including the shape, wavelength range, and broad spectral width in excess of 200 nm is a practical advantage that can be exploited.

We have demonstrated the first trial of applying a quantum interferometric technique using broadband polarization-entangled states to evaluate the PMD of a commercially available device within the telecommunications window. With the growing speed of fiber communication networks and the increasing number of discrete elements, the importance of high-resolution PMD evaluation on a component based level will likely continue to grow.

Acknowledgments

This research was supported by a grant from Capella Intelligent Subsystems, Inc.